Experimental investigation of plugging and fracturing mechanisms in unconsolidated sand reservoirs under injection of water containing suspended fine particles

Thanh Tung Nguyen, Jean Sulem, Rawaz Dlawar Muhammed, Jean-Claude Dupla, Jean Canou, Jean-Grégoire Boero-Rollo, Jalel Ochi

Experimental investigation of plugging and fracturing mechanisms in unconsolidated sand reservoirs under injection of water containing suspended fine particles

Thanh Tung Nguyen[(1)], Jean Sulem[(1)], Rawaz Dlawar Muhammed[(1)], Jean-Claude Dupla[(1)], Jean Canou[(1)], Jean-Grégoire Boero-Rollo[(2)], Jalel Ochi[(2)]

(1) Laboratoire Navier, Ecole des Ponts ParisTech, Univ. Gustave Eiffel, CNRS, Marne-la-Vallée, France

(2) TotalEnergies, Pau, France

Highlights

- A novel experimental device for radial injection of a suspension in sand specimens is developed.
- Permeability impairment and fracturing of cohesionless sand specimens are explored.
- A low particles concentration in the suspension can induce a significant injectivity loss.
- The fracturing pressure is proportional to the applied confining stress.
- Fracturing of a clogged specimen requires a higher injection pressure than an intact one and leads to a higher permeability recovery.

Abstract

Progressive plugging of the medium due to filter cake formation is considered as a major challenge during Produced Water Re-Injection (PWRI), leading decreased well injectivity during production. Field operations have shown that injectivity can be at least partially restored by fracturing the clogged medium when injecting in the frac-regime. An experimental investigation is performed to explore the effect of the injection of a suspension on the plugging and fracturing processes in an unconsolidated sand formation. The tests are performed by injecting water containing fine particles at a constant low flow rate to first clog a sand specimen (phase 1), then by increasing the flow rate until fracturing (phase 2). Experimental results exhibit a continuous increase of the injection pressure (decrease of injectivity) during phase 1 due to the formation of filter cake build-up caused by the deposition of injected solid particles. During phase 2 when the flow rate is increased, pressure drops are observed and attributed to the formation of fractures, resulting in the increase of the overall permeability of the medium. This is confirmed by post-mortem analysis of the specimens using X-ray Computed Tomography. Small radial fractures ("pseudo-cracks") induced around the injection point are visible. They appear as localized zones of higher porosity. The effect of the confining pressure and of the suspended particles concentration on the clogging and fracturing of the medium is investigated. It is shown that the clogging process strongly depends on the concentration of particles in the injected fluid. A lower quantity of injected particles is needed to induce the same level of permeability impairment when a lower concentration is used. No significant effect of particle concentration is observed on the fracturing pressure. As with pure water injection, the fracturing pressure is proportional to the imposed confining stress. Moreover, it is observed that the clogged specimen requires a higher injection pressure to reach the frac-regime as compared to an injection scenario with pure water and no filter cake formation and that permeability recovery could be higher.

Keywords: Radial injection experiments, Produced Water Re-Injection, Plugging, Fracturing, Unconsolidated sand reservoirs, X-ray Computed Tomography.

1. Introduction

During oil and gas recovery operations, a large volume of liquid waste is also generated from the production wells, of which produced water accounts for the majority, over 80% (Igunnu and Chen, 2014). The volume of produced water increases over the lifetime of production. The ratio of produced water to crude oil can be as high as 98% (Farajzadeh, 2004; Veil et al., 2004; Igunnu and Chen, 2014) depending on the nature of the oilfields, the method of drilling the wells, the different types of completion, the age of the production well (Reynolds and Kiker, 2003). Based on the evaluation of various criteria such as cost efficiency, regulatory acceptance, technical feasibility and availability of equipment, etc. Produced Water Re-Injection (PWRI) is well known as the most suitable method for handling produced water (Veil et al., 2004). Before re-injection, produced water is treated to remove organic and inorganic components (heavy metals dispersed oil, suspended solids, chemical compounds, dissolved gases and bacteria, etc.) using combined physical, chemical and biological methods (Ahmadun et al., 2009; Igunnu and Chen, 2014). However, due to treatment costs, current technology and equipment, treated produced water still contains a small amount of impurities such as solid particles of several micrometers in size and oil droplets (Sharma et al., 1997, Mainguy et al., 2020). The re-injection in the matrix regime (i.e., the injection pressure is lower than the horizontal *in-situ* stress) of treated produced water through the injection well into reservoirs leads to the clogging of the medium and consequently, loss of injectivity, due to filtration of these impurities at the reservoir inlet (Sharma et al., 1997; Al-Abduwani et al., 2005; Li and Wong, 2008; Feia et al., 2015). An experimental study conducted by Ochi and Oughanem (2018) showed that the level of plugging damage is mainly controlled by deposition of the suspended particles compared to that contributed by the deposition of oil droplets. Formation damage due to suspended particles has been extensively studied through experiments (Todd et al., 1990; Al-Abduwani et al., 2005; Feia et al., 2015) and modeling approaches (van Oort et al., 1993; Shutong and Sharma, 1997; Al-Abduwani et al., 2005; Zhou et al., 2018). Internal and external cake formations at the entrance of the medium are stated as the dominant mechanisms of formation damage (Shutong and Sharma, 1997; Feia et al., 2015).

Some treatments such as clean water injection or chemical additives injection can be performed to partially restore the permeability decline, however, these solutions are relatively expensive and only provide temporary short-term results (Sharma et al., 1997; Souilah et al., 2014; Mainguy et al., 2020). Injection or re-injection of treated produced water in the fracturing regime (i.e., when the injection pressure is higher than the horizontal *in-situ* stress) could be a reasonable solution to overcome formation damage and associated well injectivity (Ochi et al., 2014; Mainguy et al., 2020). Hydraulic fracturing is widely applied in consolidated reservoirs (i.e., rock) and its associated mechanisms are extensively described in the literature (Detournay, 2016). In contrast, fracturing of unconsolidated sand reservoirs is more difficult to achieve and not yet well mastered. Most of the previous studies of hydraulic fracturing in unconsolidated/soft sand formations were mainly related to frac-packing treatment or polymer flooding in which experiments were performed with highly viscous fluids (Bohloli and de Pater, 2006; Dong, 2010; Hurt and Germanovich, 2012) or fluids containing a very high concentration of particles (Golovin et al., 2010; Jasarevic et al., 2010). Very few studies address fracturing in PWRI situations in which the injected fluid has a very low viscosity (around 1 cP) and a low concentration of solid particles and in which the injection is maintained over

a long period of time (Onaisi et al., 2011). A literature review on this topic can be found in Nguyen (2022).

We emphasize that the subject studied in the present work concerns unconsolidated sand reservoirs for which the fracturing mechanisms are fundamentally different from those involved in fracturing soft rocks. Fracturing of soft rock formations is accompanied by the development of plastic zones at the fracture tip and fluid leak-off in the porous rock. However, the dominant mechanism of fracturing in soft rocks is tensile failure and fracture propagation is controlled by the rock toughness as studied theoretically by Sarris and Papanastasiou (2013), or experimentally in the recent paper of Yan et al. (2022). For unconsolidated sand reservoirs, the possibility of tensile failure is suppressed in favor of shear failure (Bohloli and de Pater, 2006). The formation of what appears as "pseudo-cracks" is the result of shear localization, dilation and fines transport in the granular medium as opposed to tensile fractures obtained during fracking of rock formations (Nguyen et al., 2022).

The main objectives of this paper are (1) to experimentally explore the clogging of unconsolidated sand reservoirs due to the injection of water containing suspended particles in the matrix regime and the fracturing response of the clogged specimen upon increasing the flow rate to reach the frac-regime and (2) to investigate the effect of confining pressure and particle concentration on the clogging damage and on the fracturing response of sand specimens. Finally, a comparison of the results obtained in this work with those under pure water injection presented in Nguyen et al. (2022) is proposed.

2. Experimental setup and tested materials

To mimic the PWRI operations in unconsolidated sand reservoirs, a radial injection device has been developed (Fig. 1). Details on this experimental device can be found in Nguyen et al. (2022). This setup permits a radial injection of a fluid with or without suspended particles into a cohesionless dense sand specimen of 100 mm diameter and 200 mm height under controlled constant flow rate. The specimen is prepared at a controlled density in order to obtain a permeability similar to that of *in-situ* reservoirs (about 1 Darcy).

The injection cell contains a central tube, fixed on the lower baseplate, which permits to perform a radial injection through a cylindrical specimen under imposed axial stress and confining pressure. The cell is fabricated with a limited number of metallic pieces (Fig. 2), providing a possibility to observe the granular structure of the specimen using X-ray Computed Tomography. Therefore, it is possible to visualize the entire specimen structure before and after the experiments with a very high scanning resolution. This is an important advantage of this device as compared to other setups described in the literature (Nguyen, 2022).

Fontainebleau silica sand NE34 (composed 99% of silica with D_{50} = 210 μm) and two different silica particles (C10 with D_{50} = 20 μm and C500 with D_{50} = 4.5 μm) were selected to perform the experimental program. The physical characteristics of these materials are presented in Table 1. The specimen is prepared with a mixture of NE34 sand and 10% of C10 particles in order to represent an initially damaged zone due to PWRI whereas smaller fines C500 are selected as the suspended particles carried in the injection fluid. By adjusting the amount of C10 particles, we can obtain various states of initial permeability of the specimen. The average C500 particle size (4.5 μm) in the injected fluid is within the range of that in reinjected produced water (1 to several tenths of μm as mentioned in Mainguy et al., 2020). Since the C10 and C500 particles are composed of silica, we avoid any chemical interaction with the NE34 sand. Similar compositions of the tested specimens and of the

injection fluid have been used in previous studies (Feia et al., 2015; Nguyen et al., 2022). The particle size distribution of these materials is established by laser diffraction granulometry (Fig. 3). The data given by the manufacturer allows to assess the accuracy of the measurement using this technique. The grain size distribution curves of different mixtures of NE34 + 10% C10 are also presented in Fig. 3, showing the good homogeneity and mixing repeatability of these materials (see also Nguyen et al., 2022).

3. Test procedure and specimen preparation

The complete testing procedure consists of the following steps:

- Fabrication of the specimen
- Saturation and application of the stress conditions
- Injection of water containing suspended particles at a low constant flow rate to plug the specimen and subsequent increase of the flow rate by steps until fracturing
- Injection of a small volume of dye to visualize the flow pattern after fracturing
- Scan of the specimen post-mortem using X-ray Computed Tomography
- Manual horizontal excavation of the specimen and visual observation of the fractures

Details on specimen preparation, saturation can be found in Nguyen et al. (2022).

The reconstituted specimen consists of a central injection zone and of two low permeability layers on its lower and upper parts. Two small membranes are placed between these layers in order to prevent the vertical flow out of the injection zone. Due to the presence of fine particles in the mixture and a very dense state of the N34 sand matrix ($I_{D\ NE34}$ = 0.9), manual compaction in 10 layers of 2 cm using a specific compaction groomer is applied to prepare the specimen. The surface of each compacted layer is well scarified before filling the next one to avoid segregation. The injection zone contains 10% (by mass) of C10 particles whereas the lower permeability layers contain 32% of C10 particles. The characteristics of the reference specimen are presented in Table 2. The upper and lower layers of low permeability are compacted at a lower density index of the sand matrix ($I_{D\ NE34}$ = 0.6) because of the high concentration of C10 particles (32%) in order to avoid the risk of breaking the injection tube made by PMMA material. Too strong compaction of the upper low permeability layer may also influence the density of the injection zone below. Once the specimen is fabricated, it is saturated with de-aired water. The desired stress conditions are applied under drained conditions before starting the injection process. The confining pressure is applied using an air-water pressurization cell and the axial stress is applied by the Press TRI-SCAN (Fig. 1). In drained conditions, the initial pore pressure is zero and no excess pore pressure is generated inside the specimen during the application of the initial confining and axial stresses (the sand specimen has a high permeability so that during the consolidation phase, the pore pressure does not increase). Following the observations of Benahmed (2001), the high density index of the specimen guarantees that in the range of stresses applied in the tests, the application of the confining pressure and of the axial stress does not affect the void ratio of the sample, and thus the initial permeability. During the injection test, the imposed stresses are kept constant.

The various phases of the injection process are illustrated in Fig. 4. The experiment is performed under controlled flow rate. The plugging process is simulated by first radially injecting water containing suspended particles at a constant flow rate in the matrix regime to partially clog the sand specimen (Fig. 4b), then the flow rate is increased rapidly in order to fracture this damaged specimen and to (partially)retrieve the loss of injectivity (Fig. 4c). r_0, r_c, r_1 are defined as the radius of the

injection tube, internal cake and specimen, respectively. The suspension is prepared in a 20l water tank (Fig. 1) using an efficient mixer to ensure the homogeneity of suspension in water. Fig. 5 presents a schematic diagram of the injection program with the two injection phases: plugging and fracturing. The final state of the plugging phase (phase 1) is chosen to provide a reference permeability of 80 mD before starting the fracturing phase. This permits a comparison of the critical fracturing pressure P_{frac} with that obtained in the tests with pure water injection in a specimen containing 22% of C10 particles as described in the study by Nguyen et al. (2022). Nevertheless, it is expected that the internal structure of the resulting partially clogged specimen is different from that of a homogeneous specimen prepared with 22% of C10 particles. During the fracturing phase (phase 2), the flow rate is increased by steps of 0.2 l/min (1.5 minutes for each step) until reaching the initiation of the frac-regime which is defined as first sharp pressure drop recorded at the inlet pressure transducer. Four injection steps (10 minutes for each step) are carried out in the frac-regime with the same increase of the flow rate of 0.033 l/min as the tests performed by Nguyen et al. (2022) in order to compare the increase of the permeability obtained in different injection scenarios. The injection steps in the frac-regime last longer than those in the matrix regime to track the evolution of the injection pressure after a sudden drop. At the end of the injection, a bleu dye (Basacid® Blue 762) is injected through the central tube to visualize the flow pattern within the specimen after fracturing.

4. Typical experimental results

4.1 Pore pressure evolution

Fig. 6a presents the evolution of the pore pressure for the SP1 test. For this test, the imposed confining pressure and axial stress are 200 kPa and 400 kPa respectively (Table 3). This corresponds to a stress ration K_0 of 0.5 and can represent the conditions of a reservoir at shallow depth. Pure water was initially injected at a rate of 0.2 l/min to measure the initial permeability of the specimen (Fig. 6b). The measured pressure P_1 stabilized quickly at a value of 13 kPa, corresponding to an initial permeability of 670 mD. The suspension was injected in two phases: plugging (phase 1) and fracturing (phase 2). The first one was performed at a constant flow rate of 0.2 l/min for about 6 hours until the injection fracture reached 100 kPa (Fig. 6c), corresponding to a value of the overall permeability of 80 mD which is 7.7 times smaller than the initial value. This indicates the formation of an internal cake at the entrance of the medium. This reference value of the overall permeability was chosen for easier comparison of the critical fracturing pressure of the various tests which will be detailed later in this paper.

Fig. 6d presents the change in pore pressure during phase 2. During the matrix injection regime, the flow rate was increased in steps of 0.2 l/min. Each step was maintained for approximately 1.5 min. A continuous increase in pressure was observed during these steps (see Fig. 6e) which is attributed to two phenomena: mobilization of C10 particles present in the mixture and further deposition of suspended particles in the filter cake formed during the clogging phase (see also Nguyen et al., 2022). According to Lafleur et al. (1989) the grain size distribution of the specimen containing 10% C10 (Fig. 3) is classified as the upwardly concave distribution or internally unstable distribution which is susceptible to internal erosion of fine particles in the pore network (Marot and Benamar, 2012). During injection, a small fraction of fine particles was detached and transported within the sand matrix and subsequently captured at the pore throats which results in a local clogging of the medium, and consequently, a decrease in overall permeability. This phenomenon has been widely

investigated in the literature (Skempton and Brogan, 1994; Tomlinson and Vaid, 2000; Bendahmane et al., 2008; Marot and Benamar, 2012; Chang and Zhang, 2013).

The fracturing state (i.e., the first pressure drop) was identified at a flow rate Q_{frac} of 2.23 l/min. Beyond this point, a pronounce drop of the injection pressure was observed, exhibiting a gain of the overall permeability during fracturing. Injection was carried out in the frac-regime with three more steps of 10 minutes each corresponding to a flow rate of 2.26, 2.29 and 2.33 l/min respectively then the flow rate was decreased to zero. Fig. 7a presents the evolution of the injection pressure versus the flow rate during the test. At a constant flow rate of 0.2 l/min, we observe a progressive increase of the pressure up to 100 kPa (plugging phase). Then, when increasing the flow rate, a quasi-proportional increase of the injection pressure is observed. Note that once the filter cake starts forming within the specimen, the flow pattern is not symmetrical along the injection tube anymore because of the heterogeneity of the sand pack due to deposited particles. Thus, using Darcy's law, the evaluation of the permeability from the relationship between the flow rate and the injection pressure only gives an overall equivalent permeability of the system. For this test, fracturing occurs at a critical fracturing pressure P_{frac} is 706 kPa, corresponding to 3.53 times the confining pressure. In the fracturing regime, a sharp decline of the slope of the pressure – flow rate curve is identified. When decreasing the flow rate to zero, a lower slope of pressure – flow rate curve indicates the increase in overall permeability after fracturing. Fig. 7b presents the results in terms of the apparent permeability – flow rate curve. During phase 1 at a flow rate of 0.2 l/min, the permeability decreases from 670 mD to 80 mD at the end of plugging phase. A significant increase of the permeability is observed when reaching the fracturing regime at a critical flow rate of 2.23 l/min.

To estimate the gain in permeability, denoted by g, the average values of the permeability between the matrix regime of phase 2, $k_{av,mat}$ and at the end of the test, $k_{av,unload}$ (when the flow rate is decreased) are compared based on the linear fit of the pressure – flow rate curve:

$$g = (k_{av,unload} / k_{av,mat} - 1) \times 100\ (\%) \quad (1)$$

For the SP1test, fracturing of the medium permits a gain of 41% of the overall permeability. However, the recovery is smaller than the permeability loss during the plugging phase. Note that the injection time and the flow rate play an important role in the change of permeability during this experiment (Nguyen et al., 2022).

Fig. 8 presents the results in terms of the mass of injected particles. About 0.75g of C500 injected during the plugging phase leads to a loss of 87% of the permeability. During the frac-regime, more suspended particles (about 0.9g) were injected than during the plugging phase. However, these particles did not cause a decrease of the permeability. This is mainly because of the high flow rate and of the occurrence of fractures, allowing the particles to penetrate into the medium without any further deposition on the filter cake. This observation confirms the effectiveness of produced water injection in the fracturing regime, even though a filter cake has been formed at the wellbore.

4.2 Disassembling phase

At the end of the injection phase, a small volume of a mixture of water and 0.2% blue Basacid was injected to visualize the flow pattern within the specimen. Before excavating, the specimen was scanned using X-ray CT. Fig. 9 shows some selected X-ray images at different heights of the specimen, two vertical fractures are detected near the injection tube in the upper part of the specimen (from H = 3 to H = 12 cm). These fractures are short and tortuous. To obtain a 3D view of the fractures, image processing was applied to the scans following three steps: filtering (reduction of the noise of

X-ray images), thresholding (segmentation of the fractures and the surrounding medium), volume rendering (construction of a 3D image). This process was performed using FIJI open-source software (Schindelin et al., 2012). The 3D views of two typical sections containing fractures are shown in Fig. 10. For specimen SP1, it is observed that the fractured zone is situated in the upper part. In order to obtain a good resolution of the images, we have chosen two zones (4 to 6 cm and 6 to 8 cm) with a height of 2 cm each in the central part of the specimen. From the different views of these fractures, we see that they are quite curvy in both vertical and horizontal direction.

Fig. 11 shows some views of the specimen when removing the drainage system and the external latex membrane. From the outer view (Fig. 11a), the invasion of the injected blue dye is observed only in the upper part which indicates that a higher flow occurs in this area and the fractures observed during excavation coincide with those detected in the images of the X-Ray scanned specimen (Fig. 11). Nguyen et al. (2022) have identified the fracturing mechanisms as the coupled phenomena of the formation of dilatant shear bands in the sand matrix and the subsequent transport of small particles present in these bands to form the fractures (i.e., pseudo cracks of high porosity) induced around the injection tube.

5. Sensitivity analysis

Six tests have been performed to study the effect of suspended particle concentration and of confining pressure on the formation damage by deposited particles as well as the fracturing response of sand specimens (Table 3). Then, a comparison of the results obtained with suspended particles injection with those performed under pure water injection by Nguyen et al. (2022) is proposed in order to explore the effect of the filter cake build-up at the sand surface on the fracturing of the medium.

5.1 Test repeatability

For every new experimental protocol, it is important to evaluate the repeatability of the test. A test called SP2 has been performed under the same testing conditions as the reference test (SP1). Fig. 12a,b shows a comparison of these tests during the plugging phase in terms of pressure and apparent permeability evolution. This phase was carried out at q = 0.2 l/min. A slight difference of the initial permeability was observed, depending on the initial structure of the NE34 sand and C10 particles mixture. The SP1 test showed a relatively faster increase in inlet injection pressure, corresponding to a faster decrease in overall permeability mainly due to the complexity of particle deposition, transport and rearrangement during injection.

As for the reference test, the flow rate was gradually increased in steps of 0.2 l/min until fracturing occurs. A fairly good repeatability in terms of pressure – flow rate curve is observed (Fig. 12c). In these tests, fracturing initiates when the injection pressure reaches about 3.5 times the confining pressure (Fig. 12d). During the further fracturing steps, test SP1 shows a stronger drop of the injection pressure as compared to SP2, which indicates a slightly higher increase of the overall permeability after fracturing (a gain of 41% for SP1 as compared to 22.5% for SP2).

5.2 Effect of the concentration of particles in the injection fluid

In this part, we first evaluate the impact of suspended particles concentration on the clogging of the medium and the effect of this parameter on the fracturing process is then discussed.

5.2.1 *Plugging of the medium*

Five tests (SP1, SP2, SP3, SP5 and SP6) were conducted under the same testing conditions with only the concentration of suspended particles in the injected fluid changed (10, 20 and 50 mg/l). These specimens contained a mixture of NE34 sand and 10% of C10 particles, compacted at a density index of the sand matrix $I_{D\ NE34}$ of 0.9. The stress conditions are 200 kPa confining pressure and 400 kPa axial stress. The injection was maintained constant at 0.2 l/min until the injection pressure reached a target value of 100 kPa. The results in terms of injection pressure versus injected particles mass are shown in Fig. 13a. We observe that the increase of the injection pressure is more pronounced (in terms of the quantity of injected particles) with a lower concentration of suspended particles. Similar results have been obtained by Feia et al. (2015) when investigating the effect of particles concentration on permeability impairment of a sand specimen under axial injection flow. On the contrary, when plotting the results in terms of pressure versus injected volume, it is observed that a higher concentration results in a faster increase of the injection pressure, and consequently, a faster plugging rate. Similar results were also obtained by Ochi and Oughanem (2018). Following Feia et al. (2015), this could be explained by the fact that, at a relatively low injection rate, when injecting at a lower particles concentration, the particles have time to settle on the sand grains with little re-entrainment, thus less deposited particles are needed to plug the medium. However, because of the lower concentration, a larger volume of the injected fluid is needed to provide enough deposited particles.

Test SP5 was performed with only the plugging phase in order to visualize the profile of deposited particles at the interface between specimen and injection tube (i.e., at the inlet of the medium). At the end of this test, a typical sample was carefully taken in a zone close to the injection tube and was observed using an optical microscope. As shown in Fig. 14, injected particles are captured in the porous medium to form the internal cake, consequently, reducing the overall permeability of the specimen. At this state, the external cake has not been formed yet. The results obtained validate the scenario of the cake formation before carrying out the fracturing phase in which only a filter cake is formed without the plugging of the injection tube.

5.2.2 *Fracturing of the medium*

Changing the particles concentration affects the formation of the filter cake during the plugging phase. Therefore, it may give different structures of the clogging zone, especially, around the injection point. To investigate the effect of this parameter on the fracturing process, three different concentrations have been tested (10, 20 and 50 mg/l). However, test SP6 with 50 mg/l of particles did not generate fractures because of the plugging of the injection tube due to the deposition of injected particles in the helical groove of the tube as observed during the disassembling. Therefore, we compare the results obtained in the tests with the concentration of 10 and 20 mg/l (Fig. 15). Il can be observed that the particles concentration, within the range tested, has no significant effect on the critical fracturing pressure. Fracturing occurred when the injection pressure reached about 3.45 to 3.65 times the confining pressure. Due to a sudden failure of the pump at the end of injection, test SP3 (20 mg/l) was performed with only three flow rate steps in the frac-regime (instead of four steps) (Fig. 16a), thus the increase of the apparent permeability is smaller than for the two other tests with 10 mg/l. In test SP3 (20 mg/l), fractures were generated only in the upper part of the injection zone from H = 2 cm to H = 8 cm which is shorter than for reference test SP1. This can explain the smallest increase of the overall permeability after fracturing in test SP3. Similar fracture morphology is observed in tests SP1 and SP3 (Fig. 10 and Fig. 16b).

5.3 *Effect of the confining pressure on the fracturing process.*

The experimental results with pure water injection performed by Nguyen et al. (2022) showed that the confining pressure is the primary factor controlling the fracturing pressure. It is thus interesting to investigate the effect of this parameter when injecting water with suspended particles. To do so, test SP4 was carried out at a lower confining pressure (120 kPa) as compared to the reference test (200 kPa) while keeping the same stress ratio K_0 of 0.5. The comparison is shown in Fig. 17. The higher the confining pressure, the higher the fracturing pressure and the lower the increase in permeability. Interestingly, fracturing occurs when the injection pressure reaches about 3.5 times the confining pressure for both tests. A sudden drop of the injection pressure from P_{frac} of 420 kPa to 180 kPa is observed at the critical fracturing state.

The observation of the fractures after the test is consistent with the above results. As shown in Fig. 18, a larger and more complex network of fractures is observed in specimen SP4 as compared to specimen SP1 under 200 kPa of σ_h (Fig. 10) and can be related to the strong drop of the injection pressure observed when reaching the fracturing state. During the SP1, fractures were only generated in the upper part of the specimen whereas fractures propagated all along the injection tube during test SP4. This observation is in accordance with the first noticeable fracturing point and a higher gain of the apparent permeability in test SP4 (200% of the permeability gain g for test SP4 as compared to 41% for SP1).

Nevertheless, the observation of the samples made after the experiments gives only the final state and future investigations in which scanning of the specimens could be performed during injection are needed to precisely identify the onset and propagation/coalescence of the fractures. This however, requires significant modifications of the experimental device.

5.4 *Effect of the internal cake formation on the fracturing response of the medium*

Nguyen et al. (2022) have explored fracturing mechanisms, under pure water injection, in the medium containing a homogeneous mixture of sand and fine particles which represents the final state of an internal cake induced by PWRI. In this scenario, the testing conditions can be well controlled and a homogeneous specimen allows to avoid unexpected or preferential flows within the sand specimen. The results presented in this work, on the other hand, get closer to the phenomena that occur during PWRI operations in practice with the combined phenomena: formation damage due to the formation of a filter cake on the sand surface in the matrix regime and then fracturing of the medium. However, the physical processes associated with the second scenario are more complex with the superposition and competition of several processes such as filtration, deposition, detachment, transport of fine particles and formation of dilatant deformation bands in the sand matrix.

In this part, we present a comparison of the results obtained for the two injection scenarios performed in the radial injection cell. Two test series with two different magnitudes of confining pressure (120 kPa and 200 kPa) are evaluated. The obtained results show that the injection tests with suspended particles need a higher pressure to reach the frac-regime (Fig. 19a,c). The ratio between the fracturing pressure and the confining pressure is about 3.5 for the injection of suspended particles and only 2.5 for pure water (Fig. 19b,d). With the same number of steps in the frac-regime, the suspended particles injection tests exhibit a higher recovery of permeability. This result is confirmed by the appearance of longer fractures around the injection tube as shown Fig. 20. The fracture pattern inside the clogged specimen (Scenario 2) is much more complex. Instead of propagating radially in

the flow direction from the injection tube, the fractures extend in different branches as observed in the specimen SP4.

Indeed, in Scenario 2, the fracture distribution is heterogeneous along the specimen height. Note that in the case of injection of pure water (see Nguyen et al., 2022), the fracture pattern mostly develops in the central part of the specimen. Here, when injecting a suspension, the fracture pattern is much more complex and depends upon the heterogeneity of the deposition of small particles along the height during the clogging process. Although it is observed in tests SP1 and SP3 that fractures are situated in the upper part of the sample, for SP4 they are located in the central part. No clear explanation can be drawn for the moment and further exploration of the changes induced in the granular structure of the specimen by the clogging would be needed. Interestingly, for both injection scenarios, the value of the normalized fracturing pressure (P_{frac}/σ_h) is not affected by the change of the confining pressure within the range tested here (Fig. 21).

To better understand the difference of the critical fracturing pressure, it is interesting to analyze the effect of the filter cake on the critical pressure required for fracturing. Similarly to our results, other works (Farajzadeh, 2004; Wong and Mettananda, 2010; Feia et al., 2015; Ochi and Oughanem, 2018) have shown that, during the plugging process, only the deposition of particles at the first layer (filter cake) affects the overall permeability decline of the specimen (equivalent to the increase of the inlet pressure measured at the entrance of the specimen) whereas the pressures measured at different positions within the specimen do not exhibit any significant change as illustrated in Fig. 22. ΔP_{total} and ΔP_c represent the total pressure loss and the pressure loss inside the internal cake, respectively. The presence of this cake may require a higher injection pressure to firstly break or destabilize this zone before creating fractures within the specimen. Besides the occurrence of fracturing of the specimen, the breakage or unclogging of the filter cake also plays an important role on the increase of the permeability in the frac-regime. This could explain why, after fracturing, a higher gain of the permeability can be obtained for the tests with injection of suspended particles.

6. Conclusions

In this work, an experimental study has been performed in a newly designed radial injection cell, aiming to mimic the process of re-injection of produced water in sand reservoirs in both matrix and frac-regimes.

Injection of suspended particles in the matrix regime results in a decrease in overall permeability due to the formation of an internal and/or external cake within the soil surrounding the injection tube. It is shown that when injecting at a lower particles concentration (10 mg/l), a smaller amount of injected particles (but a higher injected fluid volume) is needed to induce the same level of plugging in terms of pressure increase as compared to injecting with a higher particles concentration in the fluid (20 and 50 mg/l).

Injecting in the frac-regime, on the other hand, allows to partially restore the injectivity by breakage of the filter cake and subsequent fracturing of the medium. Moreover, in the frac-regime, it is possible to continue to inject the suspension without further deterioration of the overall permeability. An increase of the confining pressure (from 120 kPa to 200 kPa) leads to a proportional increase of the critical fracturing pressure. For the range of particles concentration studied (10 and 20 mg/l), no clear effect of this parameter was observed on both the fracturing pressure and the fracture geometry. In all the tests, fracturing occurred when the injection pressure reached about 3.5 times the confining pressure.

It is interesting to compare the results of two injection scenarios: injection of pure water as performed by Nguyen et al. (2022) and injection of water with suspended particles. The second scenario exhibits a higher normalized fracturing pressure (P_{frac}/σ_h). In the frac regime, a higher gain of the permeability can be obtained and longer fractures are observed. These observations highlight the effect of the filter cake: The fracturing process involves both the breakage of the cake and the formation of fractures inside the specimen. In both injection scenarios, a higher confining pressure leads to a higher critical fracturing pressure, a lower increase of overall permeability as well as shorter fractures induced within the specimen.

This experimental work will be extended in the future by performing the injection tests in a large injection device to better simulate reservoir conditions and to explore the size effect on the fracturing conditions.

Declaration of competing interest

The authors declare no competing financial interest.

Acknowledgements

The authors gratefully acknowledge TotalEnergies for financial support and permission to publish this work. They are also grateful to Dr. Michel Bornert and Dr. Patrick Aimedieu for their useful comments and suggestions for the X-ray CT study.

References

Ahmadun, F.-R., Pendashteh, A., Abdullah, L.C., Biak, D.R.A., Madaeni, S.S., Abidin, Z.Z., 2009. Review of technologies for oil and gas produced water treatment. J. Hazard. Mater. 170, 530–551. https://doi.org/10.1016/j.jhazmat.2009.05.044

Al-Abduwani, F.A.., Shirzadi, A., van den Broek, W.M.G.T., Currie, P.K., 2005. Formation damage vs. solid particles deposition profile during laboratory-simulated produced-water reinjection. SPE J. 10, 138–151. https://doi.org/10.2118/82235-pa

Al-Abduwani, F.A.H., Hime, G., Alvarez, A., Farajzadeh, R., 2005. New experimental and modelling approach for the quantification of internal filtration, in: SPE European Formation Damage Conference. OnePetro. https://doi.org/10.2118/94634-ms

Benahmed, N., 2001. Comportement mécanique d'un sable sous cisaillement monotone et cyclique : application aux phénomènes de liquéfaction et de mobilité cyclique. PhD Thesis, Ecole Nationale des Ponts et Chaussées (in French).

Bendahmane, F., Marot, D., Alexis, A., 2008. Experimental parametric study of suffusion and backward erosion. J. Geotech. geoenvironmental Eng. 134, 57–67.

Bohloli, B., de Pater, C.J., 2006. Experimental study on hydraulic fracturing of soft rocks: Influence of fluid rheology and confining stress. J. Pet. Sci. Eng. 53, 1–12. https://doi.org/10.1016/j.petrol.2006.01.009

Chang, D.S., Zhang, L.M., 2013. Critical hydraulic gradients of internal erosion under complex stress states. J. Geotech. Geoenvironmental Eng. 139, 1454–1467. https://doi.org/10.1061/(asce)gt.1943-5606.0000871

Detournay, E., 2016. Mechanics of Hydraulic Fractures. Annu. Rev. Fluid Mech. 48, 311–339. https://doi.org/10.1146/annurev-fluid-010814-014736

Dong, Y., 2010. Hydraulic fracture containment in sand. Delft University of Technology.

Farajzadeh, R., 2004. Produced Water Re-Injection (PWRI): An experimental investigation into internal filtration and external cake build up. Delft Univ. Technol.

Feia, S., Dupla, J.C., Ghabezloo, S., Sulem, J., Canou, J., Onaisi, A., Lescanne, H., Aubry, E., 2015. Experimental investigation of particle suspension injection and permeability impairment in porous media. Geomech. Energy Environ. 3, 24–39. https://doi.org/10.1016/j.gete.2015.07.001

Golovin, E., Jasarevic, H., Chudnovsky, A., Dudley, J.W., Wong, G.K., 2010. Observation and characterization of hydraulic fracture in cohesionless sand, in: 44th US Rock Mechanics Symposium and 5th US-Canada Rock Mechanics Symposium. OnePetro.

Hurt, R.S., Germanovich, L.N., 2012. Parameters controlling hydraulic fracturing and fracture tip-dominated leakoff in unconsolidated sands, in: SPE Annual Technical Conference and Exhibition. OnePetro, pp. 1–19. https://doi.org/10.2118/160140-MS

Igunnu, E.T., Chen, G.Z., 2014. Produced water treatment technologies. Int. J. Low-Carbon Technol. 9, 157–177. https://doi.org/10.1093/ijlct/cts049

Jasarevic, H., Golovin, E., Chudnovsky, A., Dudley, J.W., Wong, G.K., 2010. Observation and modeling of hydraulic fracture initiation in cohesionless sand, in: 44th US Rock Mechanics Symposium and 5th US-Canada Rock Mechanics Symposium. OnePetro.

Lafleur, J., Mlynarek, J., Rollin, A.L., 1989. Filtration of broadly graded cohesionless soils. J. Geotech. Eng. 115, 1747–1768.

Li, Z., Wong, R.C.K., 2008. Estimation of suspended particle retention rate and permeability damage in sandstone from back analysis of laboratory injection tests, in: Canadian International Petroleum Conference. OnePetro.

Mainguy, M., Perrier, S., Buré, E., 2020. Produced-Water Reinjection in Deep Offshore Miocene Reservoirs, Block 17, Angola. SPE Prod. Oper. 35, 292–307. https://doi.org/10.2118/197061-PA

Marot, D., Benamar, A., 2012. Suffusion, transport and filtration of fine particles in granular soil, Erosion of Geomaterials. https://doi.org/10.1002/9781118561737.ch2

Nguyen, T.T., 2022. Experimental study of fracturing mechanisms in unconsolidated sand reservoirs under fluid injection. Ecole des Ponts ParisTech.

Nguyen, T.T., Sulem, J., Muhammed, R.D., Dupla, J.-C., Canou, J., Boero-Rollo, J.-G., Ochi, J., 2022. An experimental setup with radial injection cell for investigation of fracturing in unconsolidated sand reservoirs under fluid injection. J. Pet. Sci. Eng. 213, 110362. https://doi.org/10.1016/j.petrol.2022.110362

Ochi, J., Dexheimer, D., Corpel, P. V., 2014. Produced-water-reinjection design and uncertainties assessment, in: SPE Production and Operations. pp. 192–203. https://doi.org/10.2118/165138-PA

Ochi, J., Oughanem, R., 2018. An experimental investigation of formation damage induced by PWRI in unconsolidated sands, in: SPE International Symposium on Formation Damage Control. https://doi.org/10.2118/189513-ms

Onaisi, A., Ochi, J., Mainguy, M., Souillard, P., 2011. Modeling non-matrix flow and seals integrity in soft sand reservoirs, in: SPE European Formation Damage Conference. Society of Petroleum Engineers, pp. 1371–1387.

Reynolds, R.R., Kiker, R.D., 2003. Produced water and associated issues, Oklahoma Geological Survey.

Sarris, E., Papanastasiou, P., 2013. Numerical modeling of fluid-driven fractures in cohesive poroelastoplastic continuum. Int. J. Numer. Anal. Methods Geomech. 37, 1822–1846. https://doi.org/10.1002/nag

Schindelin, J., Arganda-Carreras, I., Frise, E., Kaynig, V., Longair, M., Pietzsch, T., Preibisch, S., Rueden, C., Saalfeld, S., Schmid, B., Tinevez, J.Y., White, D.J., Hartenstein, V., Eliceiri, K., Tomancak, P., Cardona, A., 2012. Fiji: An open-source platform for biological-image analysis. Nat. Methods 9, 676–682. https://doi.org/10.1038/nmeth.2019

Sharma, M.M., Pang, S., Wennberg, K.E., Morgenthaler, L.N., 1997. Injectivity decline in water-injection wells: An offshore Gulf of Mexico case study, in: SPE European Formation Damage Conference. OnePetro. https://doi.org/10.2118/60901-PA

Shutong, P., Sharma, M.M., 1997. A model for predicting injectivity decline in water-injection wells, in: SPE Formation Evaluation. pp. 194–201.

Skempton, A.W., Brogan, J.M., 1994. Experiments on piping in sandy gravels. Géotechnique 44, 449–460.

Souilah, R., Brocart, B., Ourir, A., Onaisi, A., Pourpak, H., Ochi, J., Lescanne, H., 2014. Produced water re-injection in a deep offshore environment-Angola block 17, in: SPE - European Formation Damage Conference, Proceedings,. OnePetro. https://doi.org/10.2118/168216-ms

Todd, A.C., Kumar, T., Mohammadi, S., 1990. Value and analysis of core-based water-quality experiments as related to water injection schemes. SPE Form. Eval. 5. https://doi.org/10.2118/17148-pa

Tomlinson, S.S., Vaid, Y.P., 2000. Seepage forces and confining pressure effects on piping erosion. Can. Geotech. J. 37, 1–13. https://doi.org/10.1139/t99-116

van Oort, E., van Velzen, J.F.G., Leerlooijer, K., 1993. Impairment by suspended solids invasion. Testing and prediction. SPE Prod. Facil. 8, 178–183. https://doi.org/10.2118/23822-pa

Veil, J.A., Puder, M.G., Elcock, D., Redweik Jr, R.J., 2004. A white paper describing produced water from production of crude oil, natural gas, and coal bed methane.

Wong, R.C.K., Mettananda, D.C.A., 2010. Permeability reduction in Qishn sandstone specimens due to particle suspension injection. Transp. porous media 81, 105–122. https://doi.org/10.1007/s11242-009-9387-0

Yan, C., Chen, Y., Chen, T., Cheng, Y., Yan, X., 2022. Experimental Study of Hydraulic Fracturing for Unconsolidated Reservoirs. Rock Mech. Rock Eng. 55, 3399–3424. https://doi.org/10.1007/s00603-022-02827-6

Zhou, K., Hou, J., Sun, Q., Guo, L., Bing, S., Du, Q., Yao, C., 2018. A Study on Particle Suspension Flow and Permeability Impairment in Porous Media Using LBM–DEM–IMB Simulation Method. Transp. Porous Media 124, 681–698. https://doi.org/10.1007/s11242-018-1089-z

List of Symbols

Symbol	Units	Definition
$I_{D\ NE34}$		Density index of the NE34 sand matrix
k	Darcy	Intrinsic permeability
$k_{av,mat}$	Darcy	Average permeability of specimen during the matrix regime
$k_{av,unload}$	Darcy	Average permeability of specimen during the unloading phase
K_0		Stress ratio coefficient
g	%	Gain of the permeability after fracturing
p	kPa	Pressure
P_1	kPa	Measured pressure by the inlet pressure transducer
P_2	kPa	Measured pressure by the outlet pressure transducer
P_{frac}	kPa	First drop pressure observed during fracturing regime
P_{in}	kPa	Pressure at the entrance of injection tube
q	l/min	Flow rate
Q_{frac}	l/min	Flow rate corresponding to the first drop pressure
t	min	Time
σ_h	kPa	Confining pressure
σ_v	kPa	Axial stress

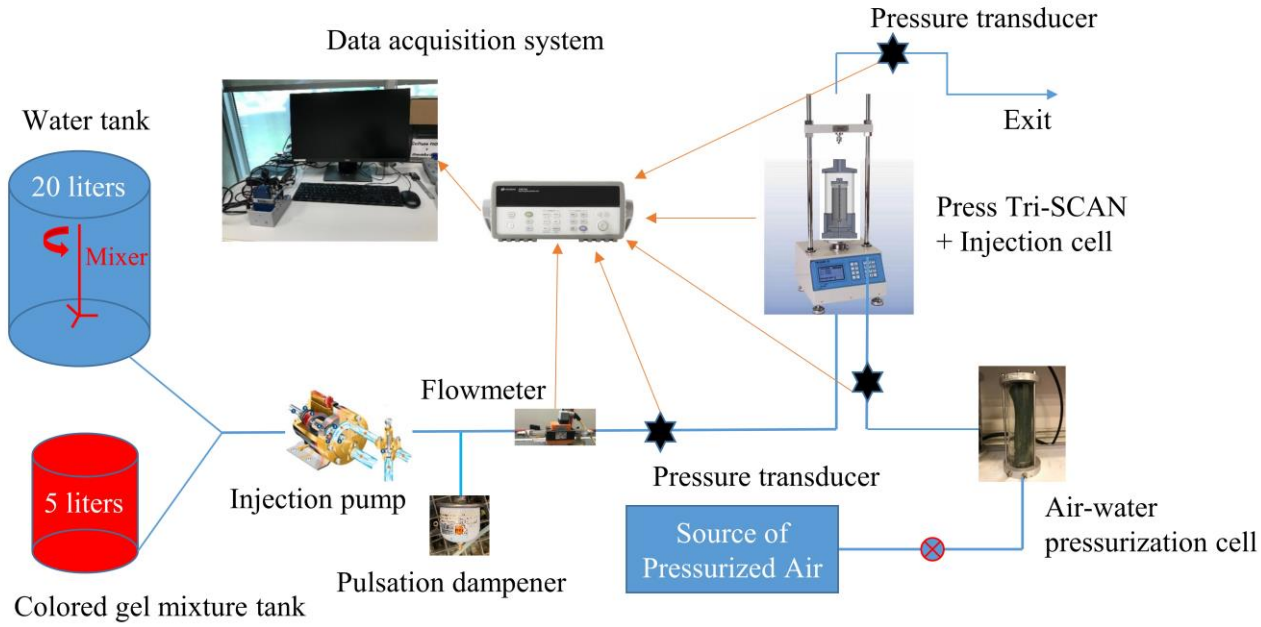

Fig. 1: Functional scheme of the radial injection cell setup (after Nguyen et al., 2022).

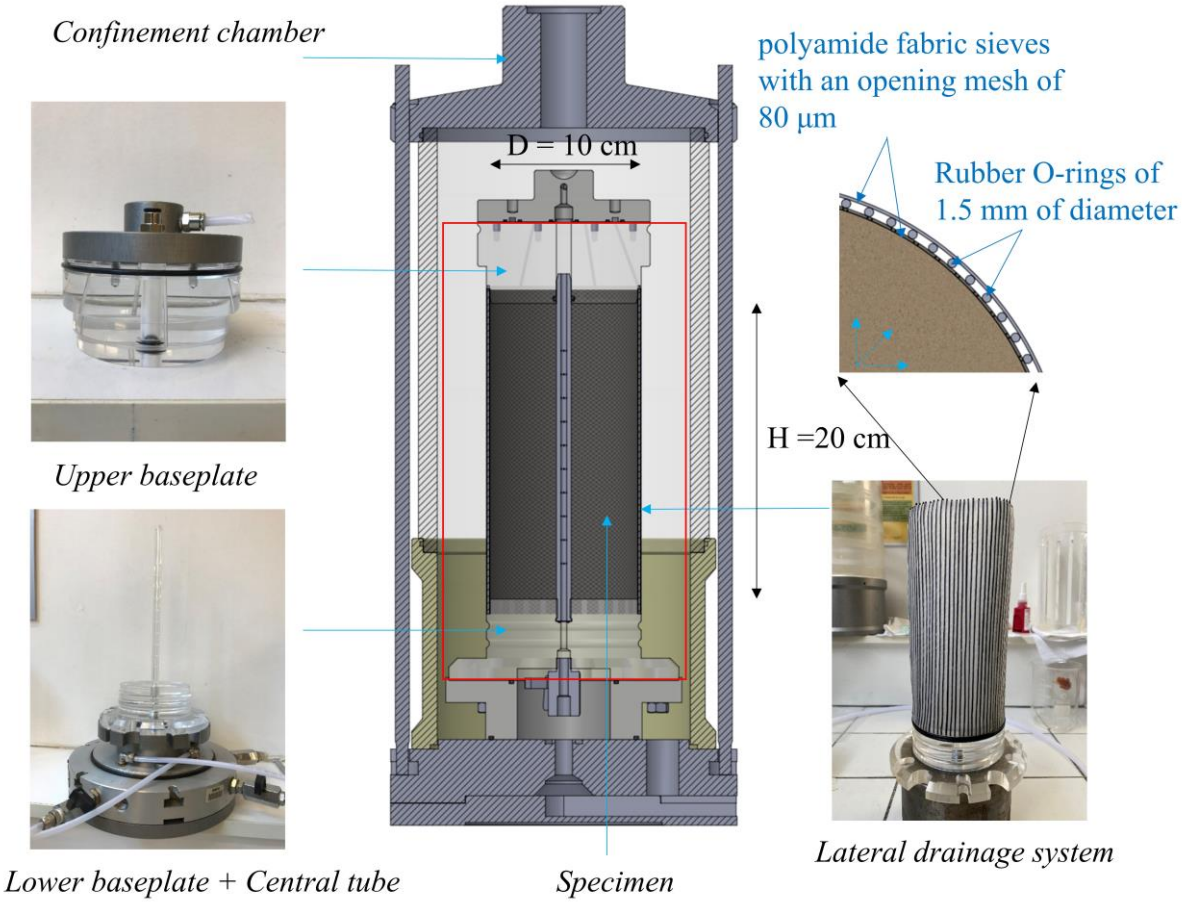

Fig. 2: 2D cross section of the radial injection cell and its corresponding components (from Nguyen et al., 2022).

562

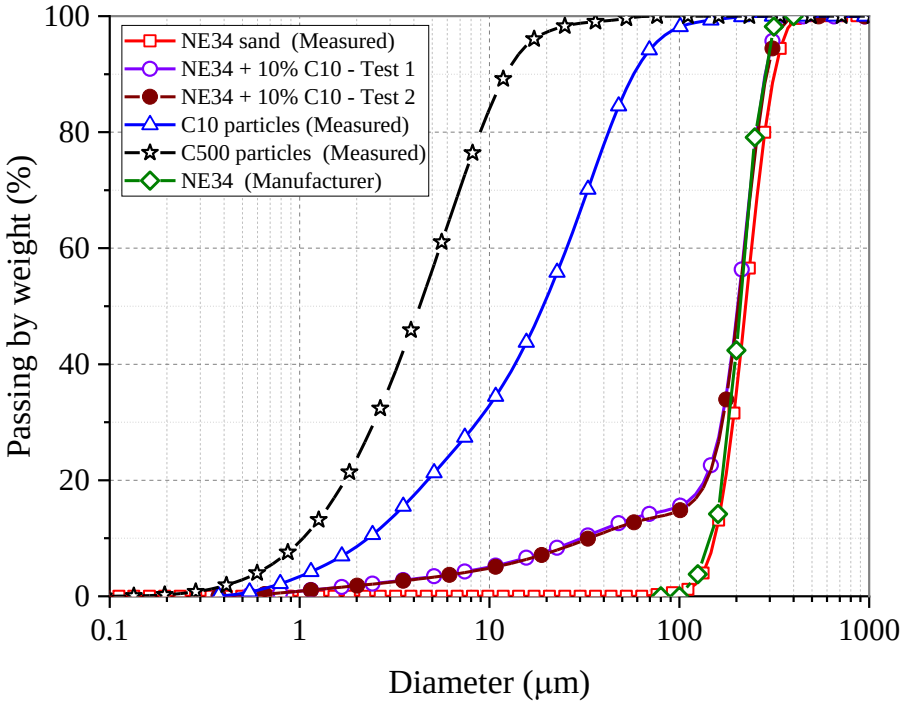

563

564 Fig. 3: Grain size distribution of the tested materials.

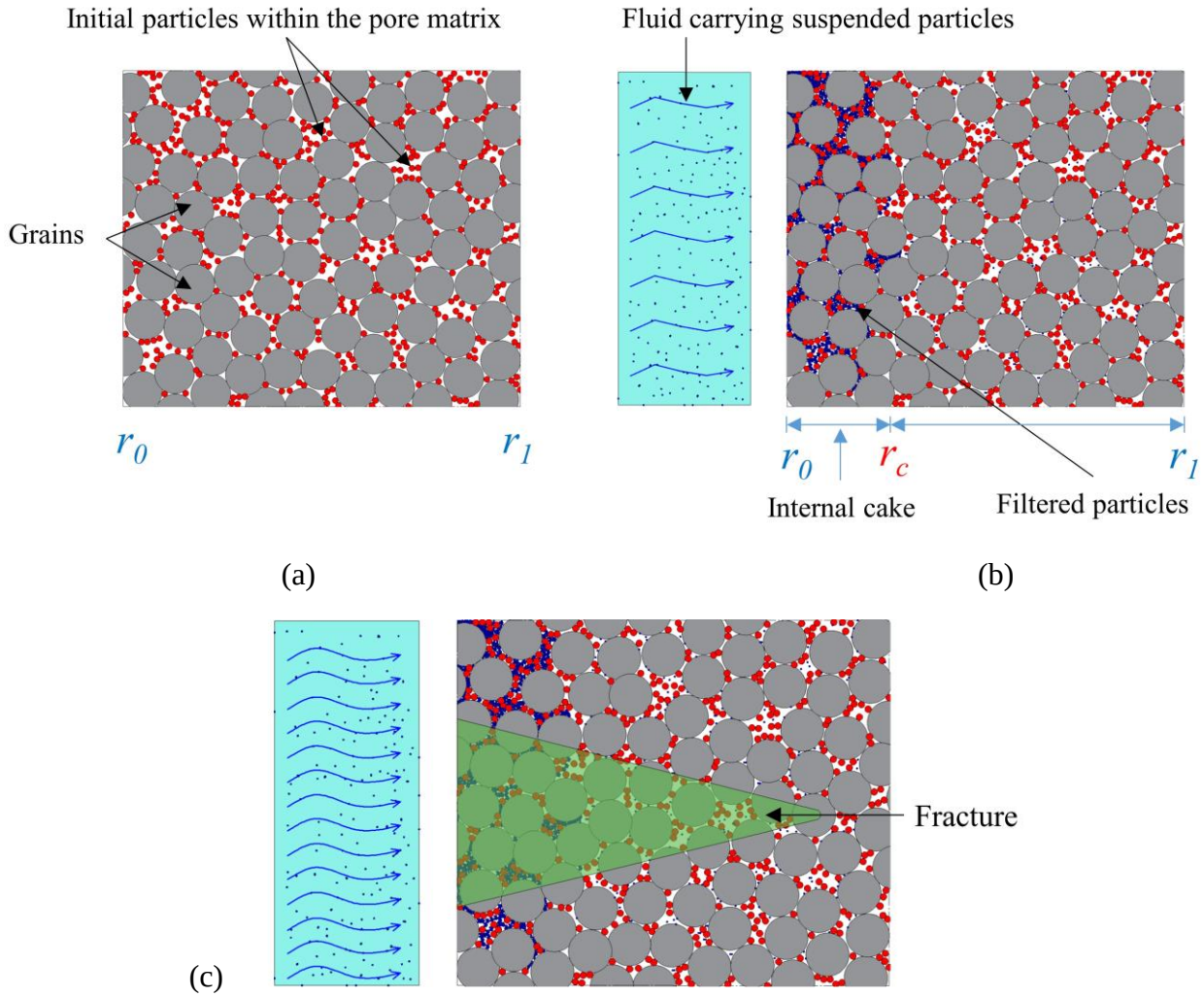

Fig. 4: Various phases of the injection process: (a) initial state of the specimen; (b) plugging of the medium due to the deposition of suspended particles; (c) fracturing of the clogged specimen under high injection pressure.

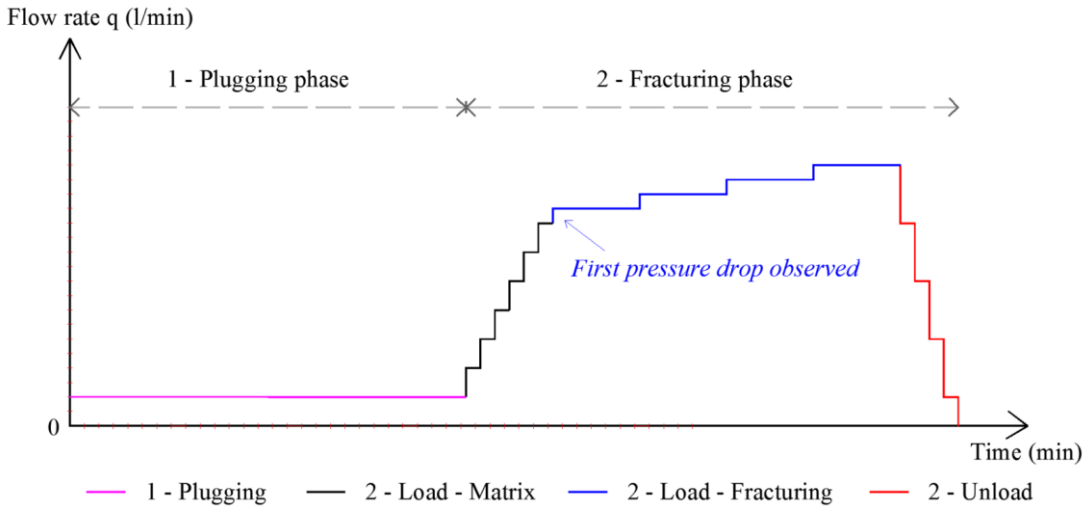

Fig. 5: Scheme of the injection program with two injection phases: plugging and fracturing

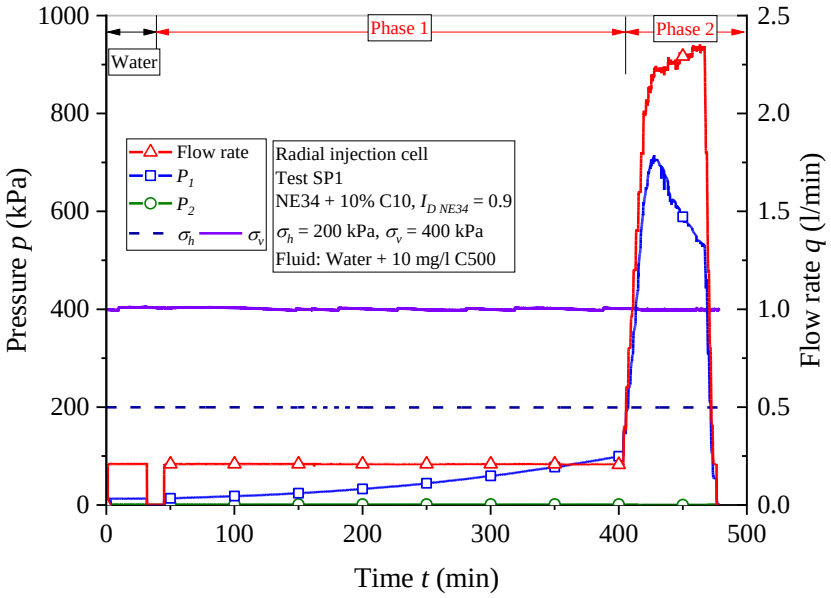

(a)

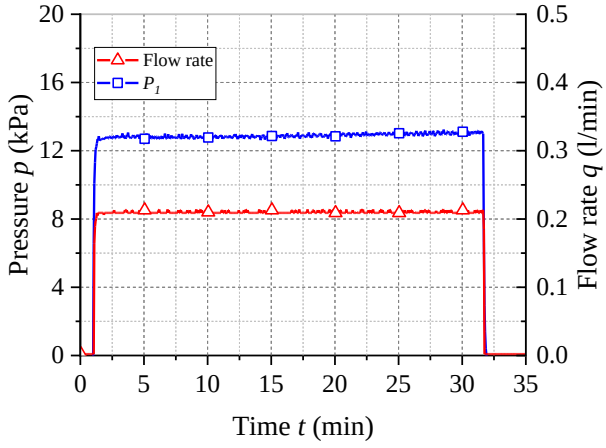

(b)

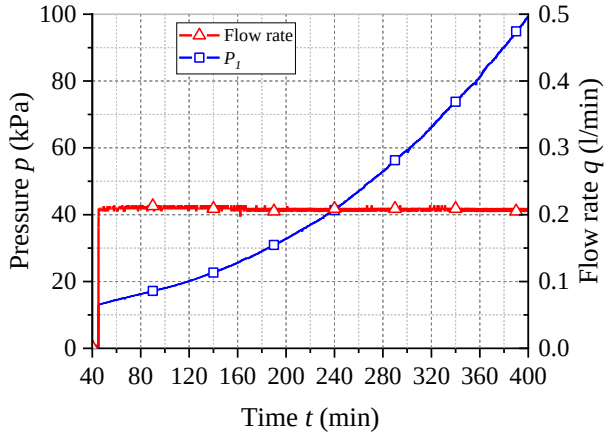

(c)

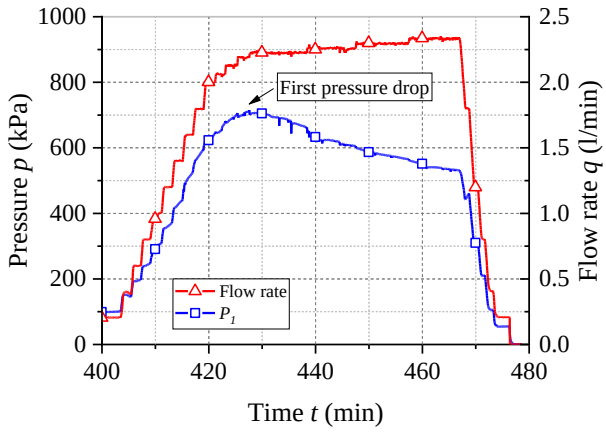

(d)

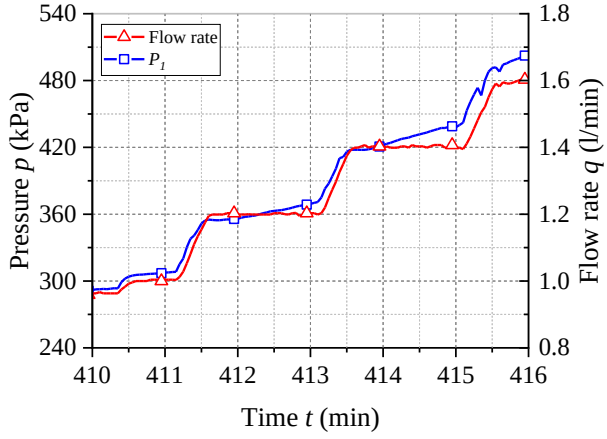

(e)

Fig. 6: Experimental results of test SP1: (a) full response; (b) initial step of pure water injection; (c) phase 1 of suspended particles injection at a constant flow rate of 0.2 l/min; (d) phase 2 with a loading – unloading cycle of flow rate; (e) increase of the injection pressure in the matrix injection regime.

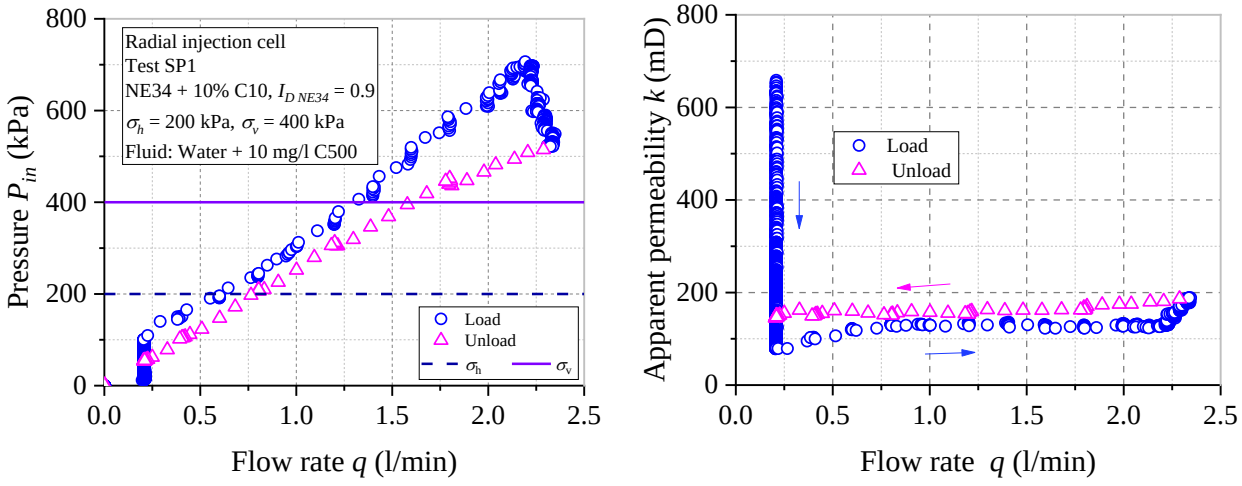

(a) (b)

Fig. 7: Results of test SP1 (a) evolution of pressure; (b) evolution of apparent permeability.

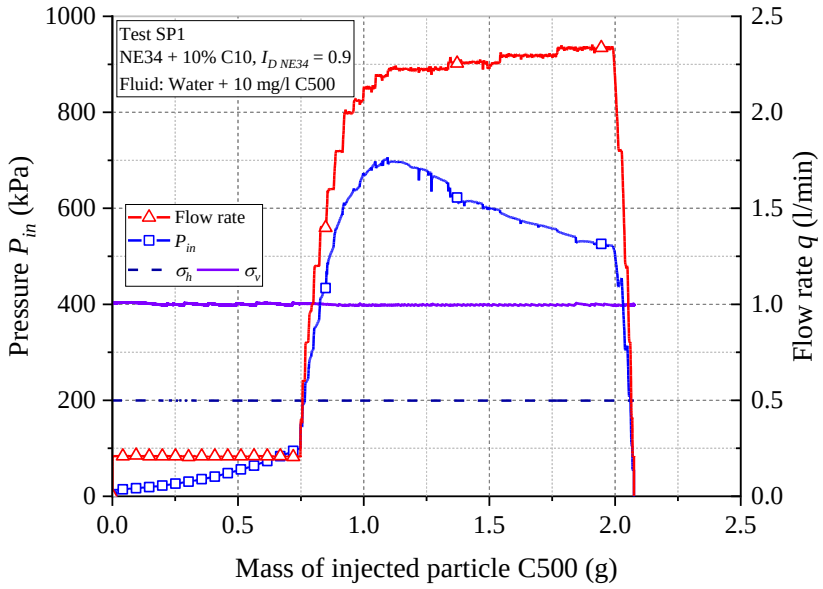

Fig. 8: Cumulative mass of injected C500 particles during the experiment SP1.

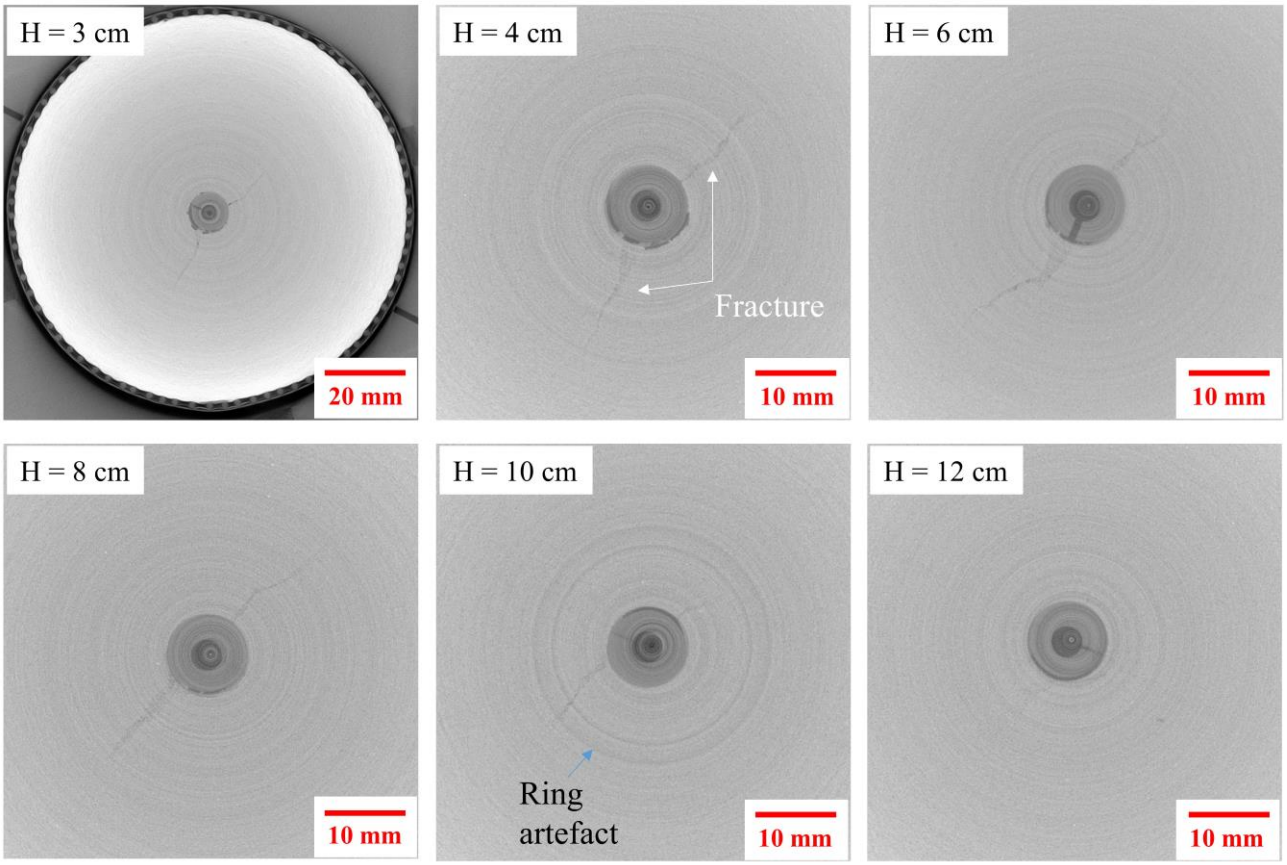

584

585 Fig. 9: Selected X-ray CT images at different heights of specimen SP1.

586

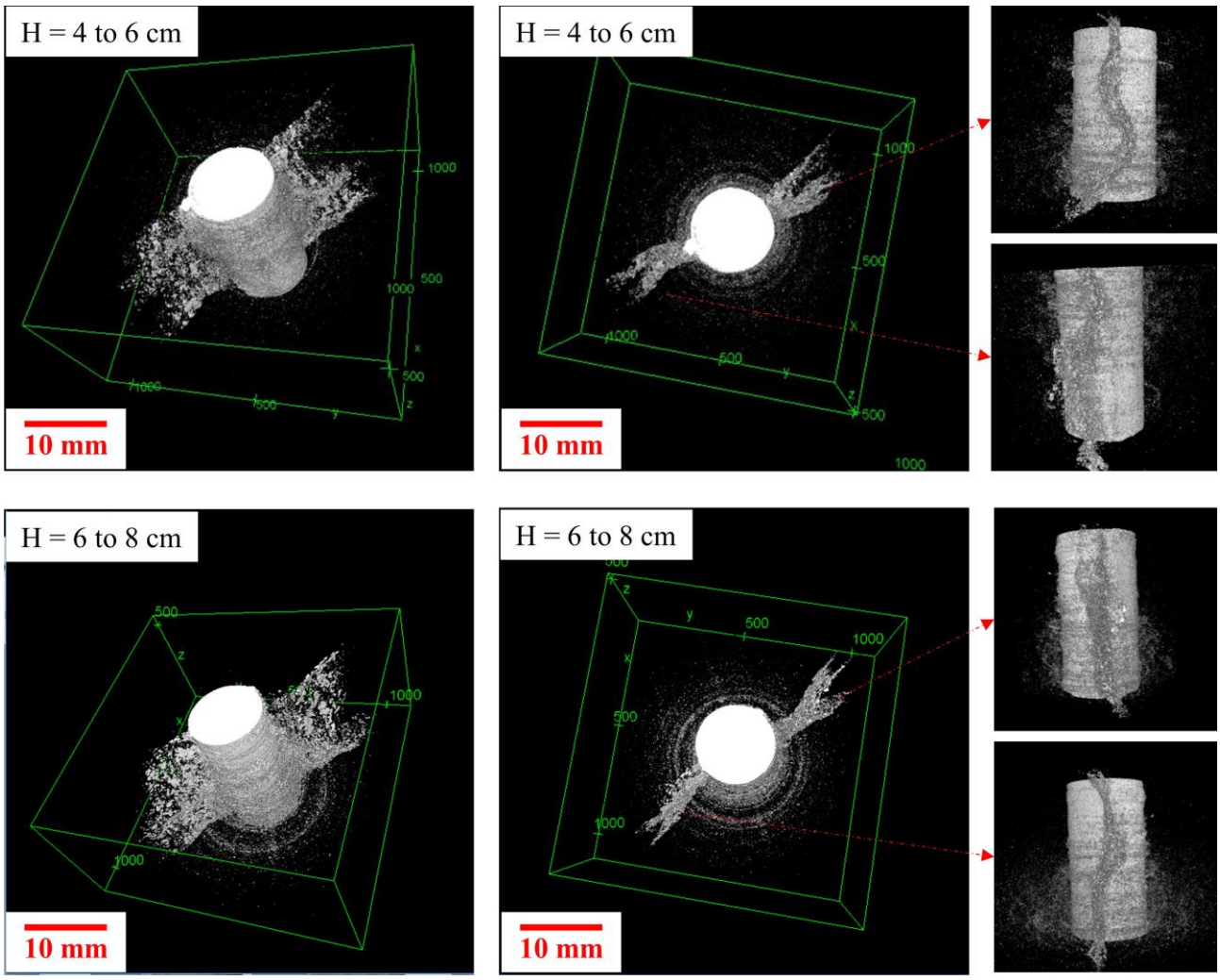

587

588 Fig. 10: 3D views of fractures developed along two different sections of specimen SP1: Section 1
589 from H = 4 to 6 cm and Section 2 from H = 6 to 8 cm.

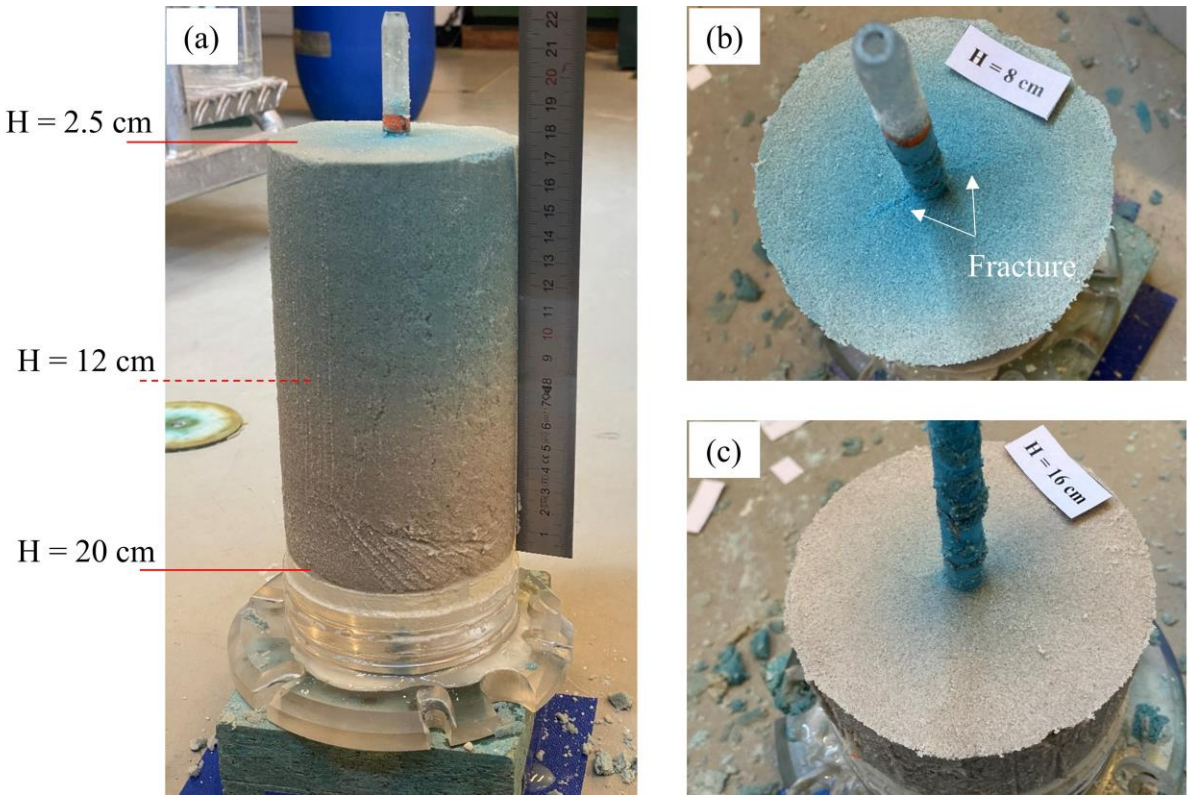

590

591 Fig. 11: Views of the specimen post-mortem: (a) global view; (b) and (c) horizontal cross-section at
592 H = 8 cm and H = 16 cm respectively.

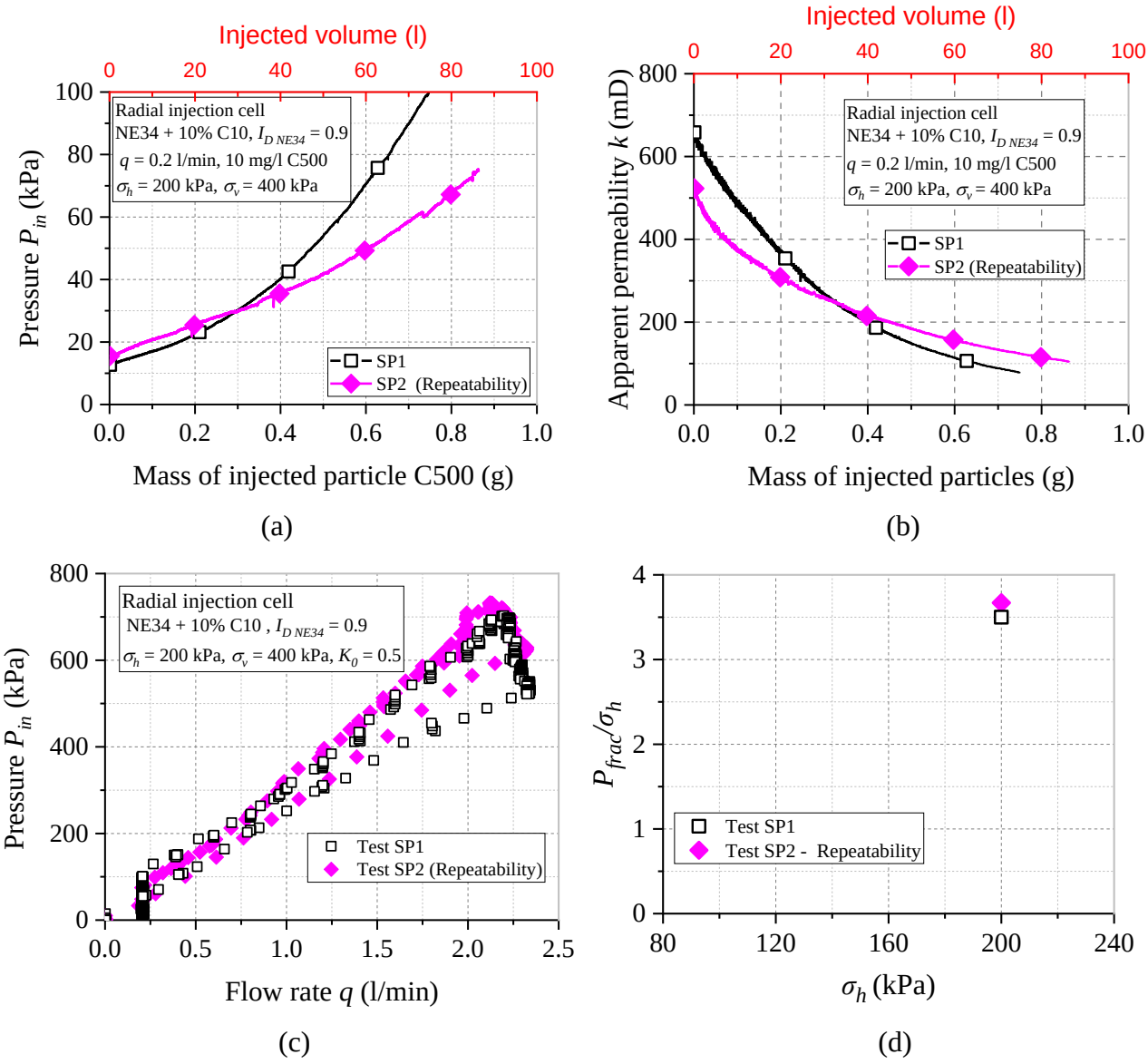

Fig. 12: Repeatability tests during the plugging phase: (a) evolution of the injection pressure (b) apparent permeability and during fracturing phase: (c) pressure – flow rate curve; (d) normalized fracturing pressure (P_{frac}/σ_h).

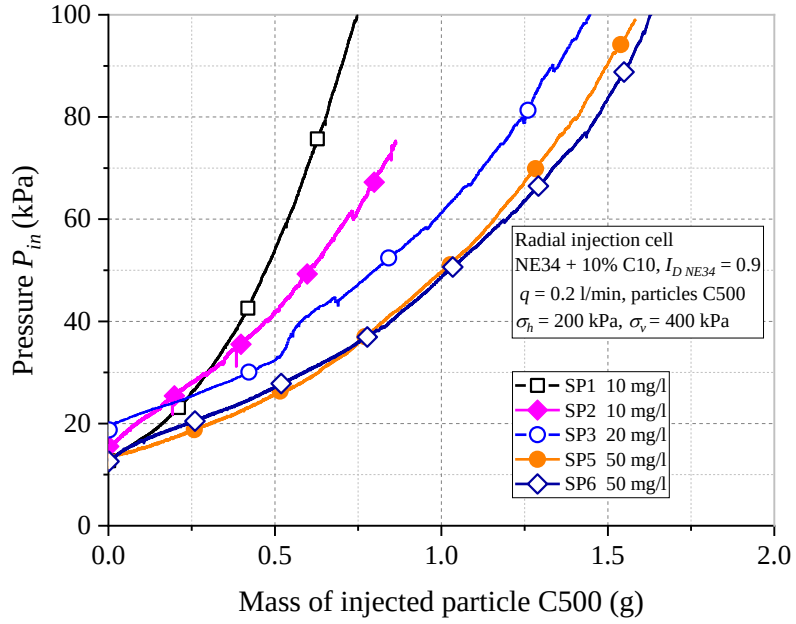

(a)

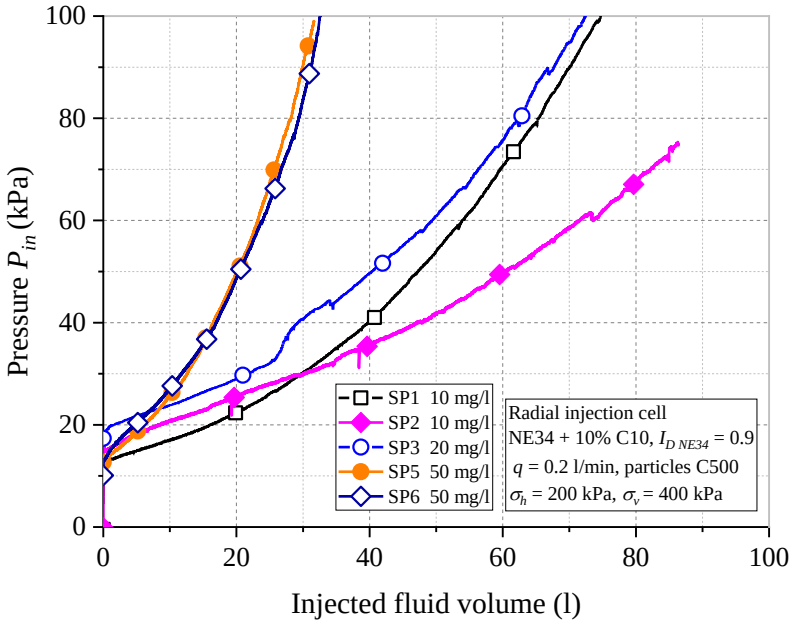

(b)

Fig. 13: Effect of the particles concentration on the plugging damage: (a) injection pressure versus mass of injected particles and (b) injection pressure versus injected fluid volume.

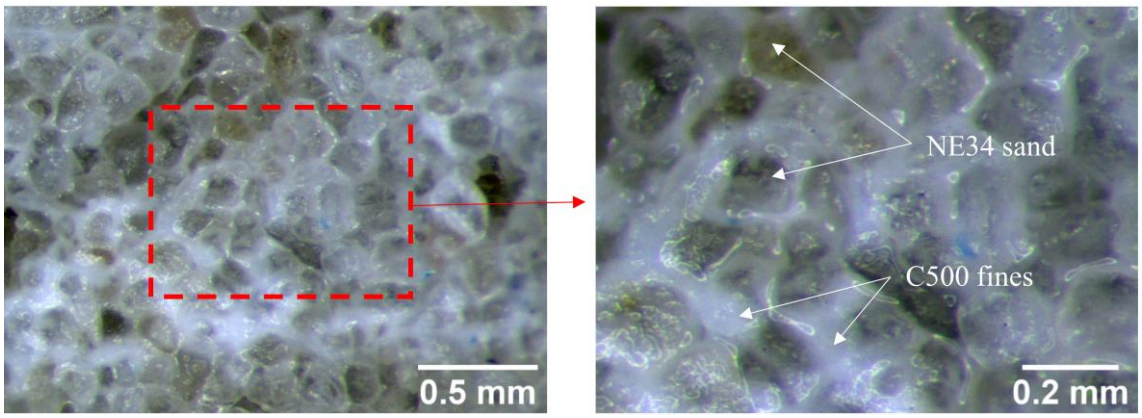

Fig. 14: Test SP5 - Optical microscope observation of the interface between specimen and 80 µm sieve covered the injection tube.

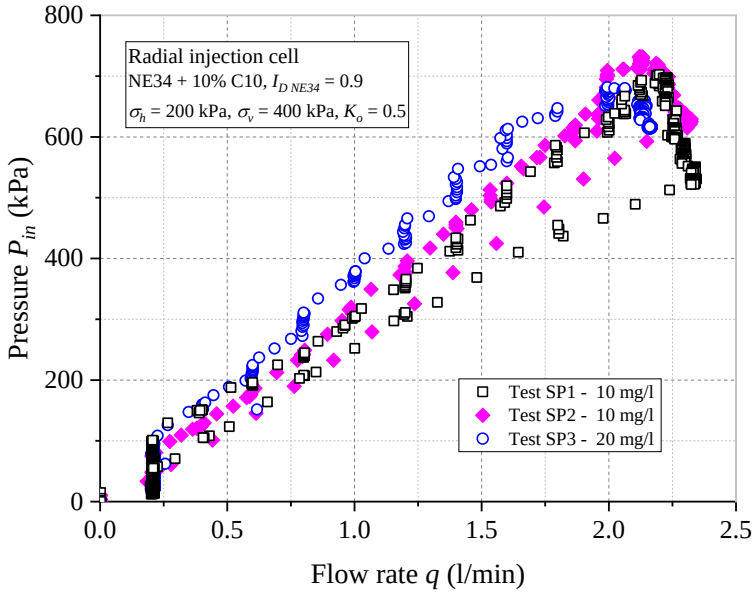

Fig. 15: Effect of the particles concentration on the fracturing response.

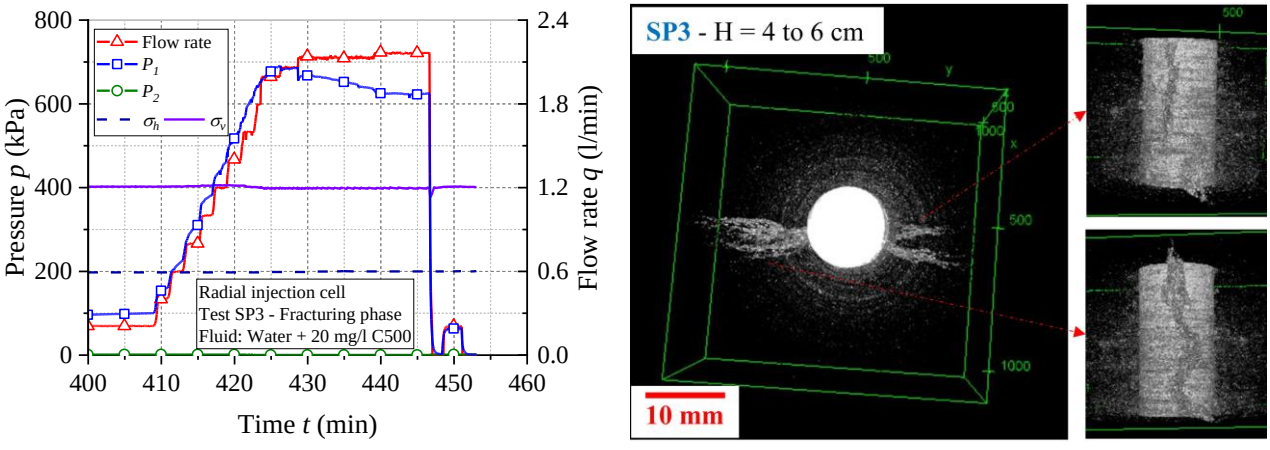

(a) (b)

Fig. 16: Test SP3 (a) injection results during phase 2 (fracturing phase); (b) 3D views of the fractures induced along a section between H = 4 cm and H = 6 cm.

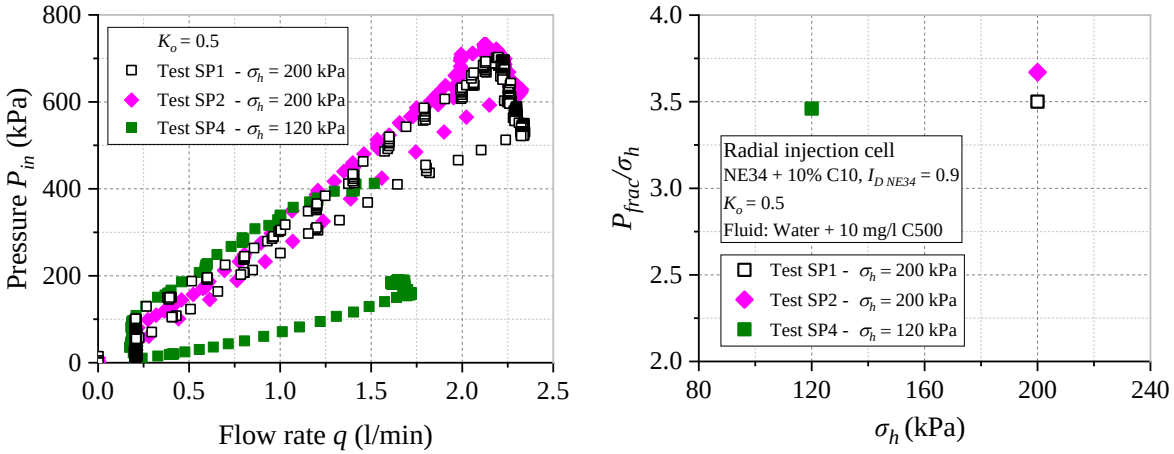

(a) (b)

Fig. 17: Effect of the confining pressure on the fracturing response: (a) injection pressure versus flow rate; (b) normalized fracturing pressure.

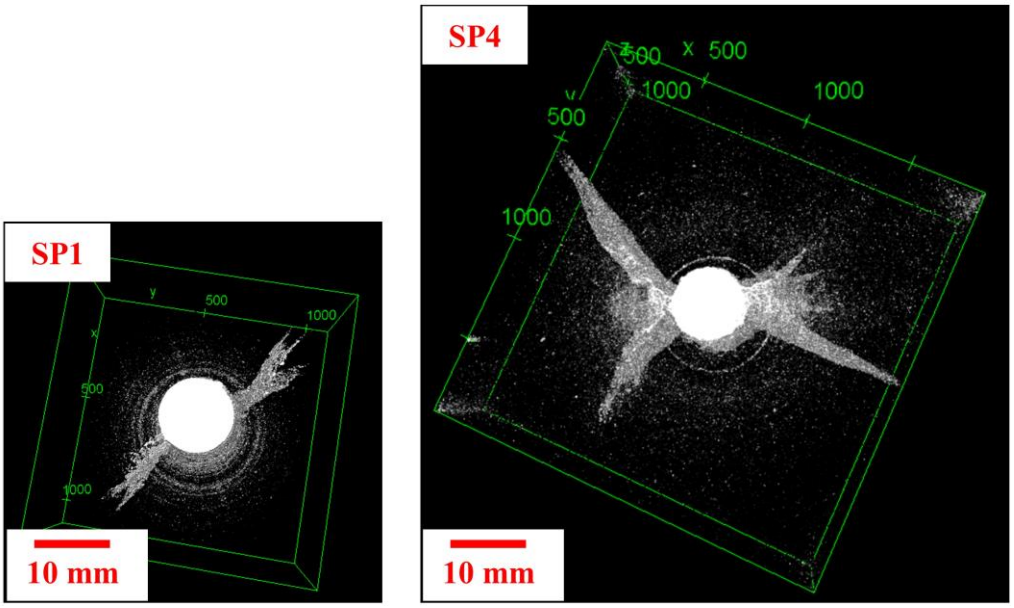

Fig. 18: 3D views of the fractures developed at the center of the specimens SP1 and SP4.

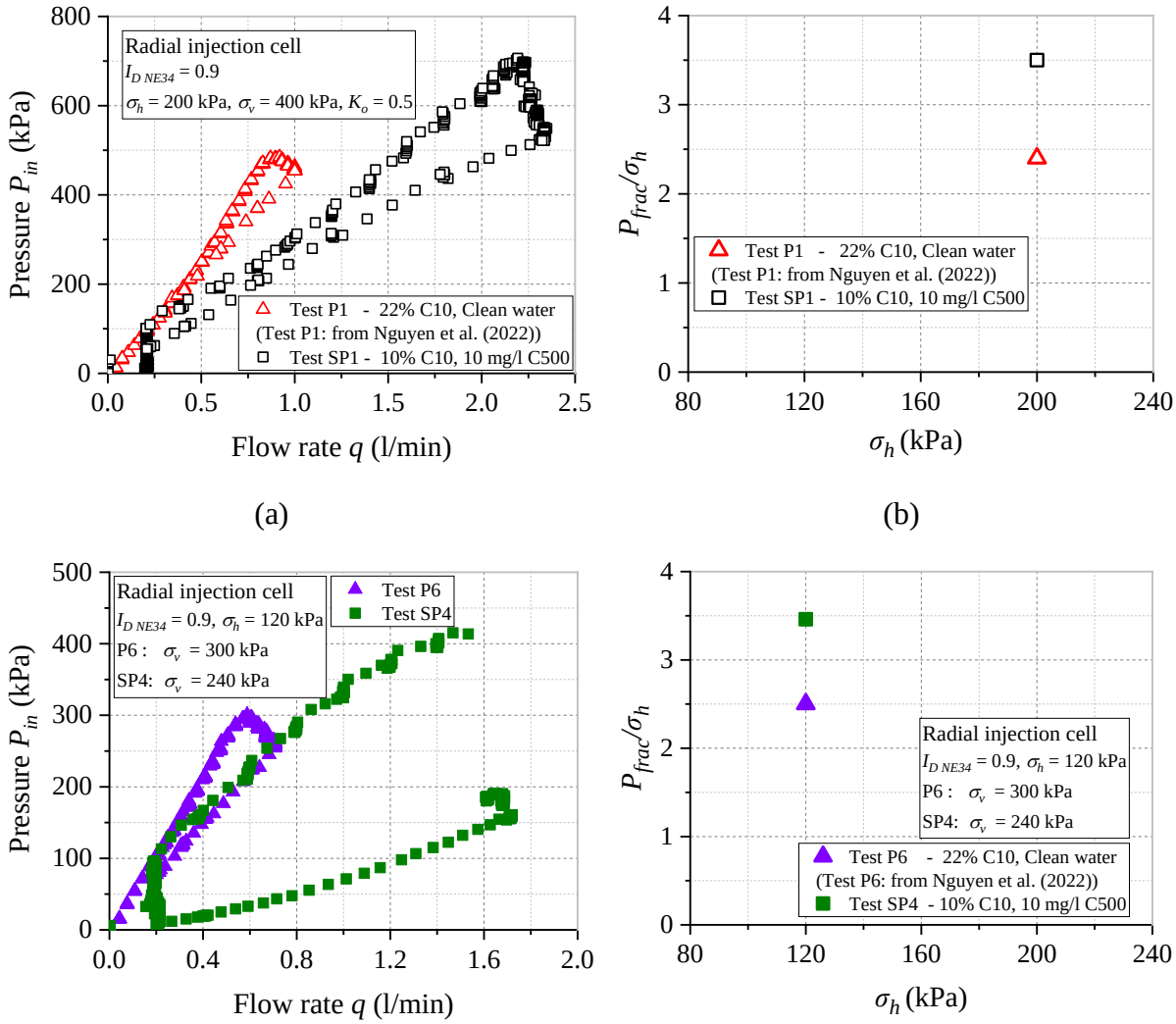

Fig. 19: Results comparison of two injection scenarios (pure water: Nguyen et al., 2022) and water containing suspended particles) at the same stress conditions: (a) and (c) injection pressure versus flow rate; (b) and (d) normalized fracturing pressure (P_{frac}/σ_h).

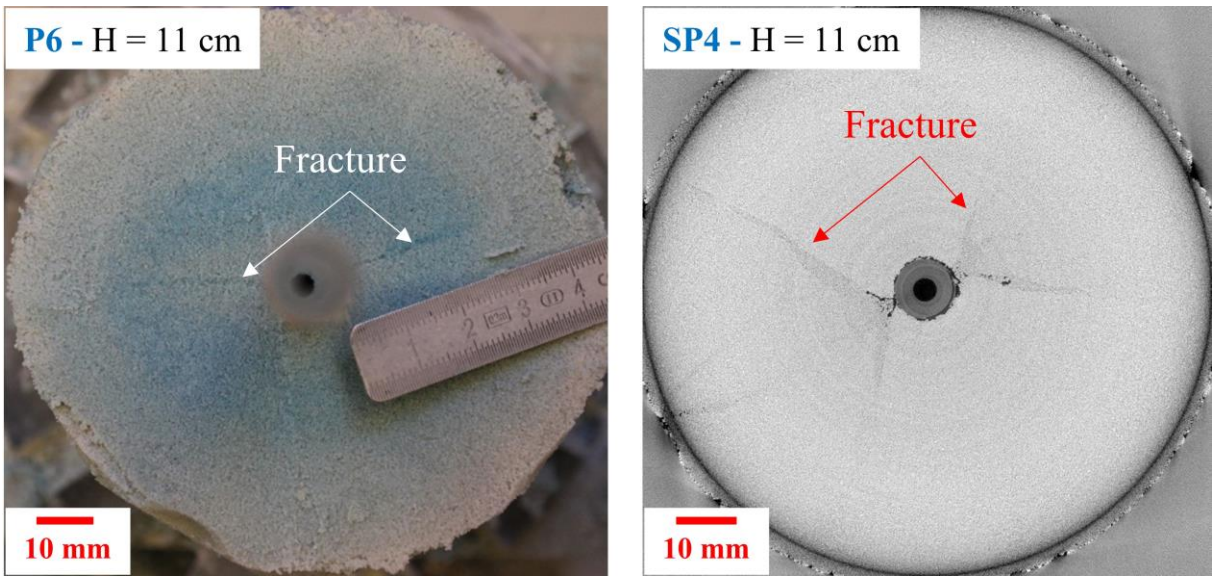

Fig. 20: Typical fracture patterns observed in two scenarios at the same confining pressure of 120 kPa (Pure water – Test P6: Nguyen et al., 2022), Suspended particles – Test SP4).

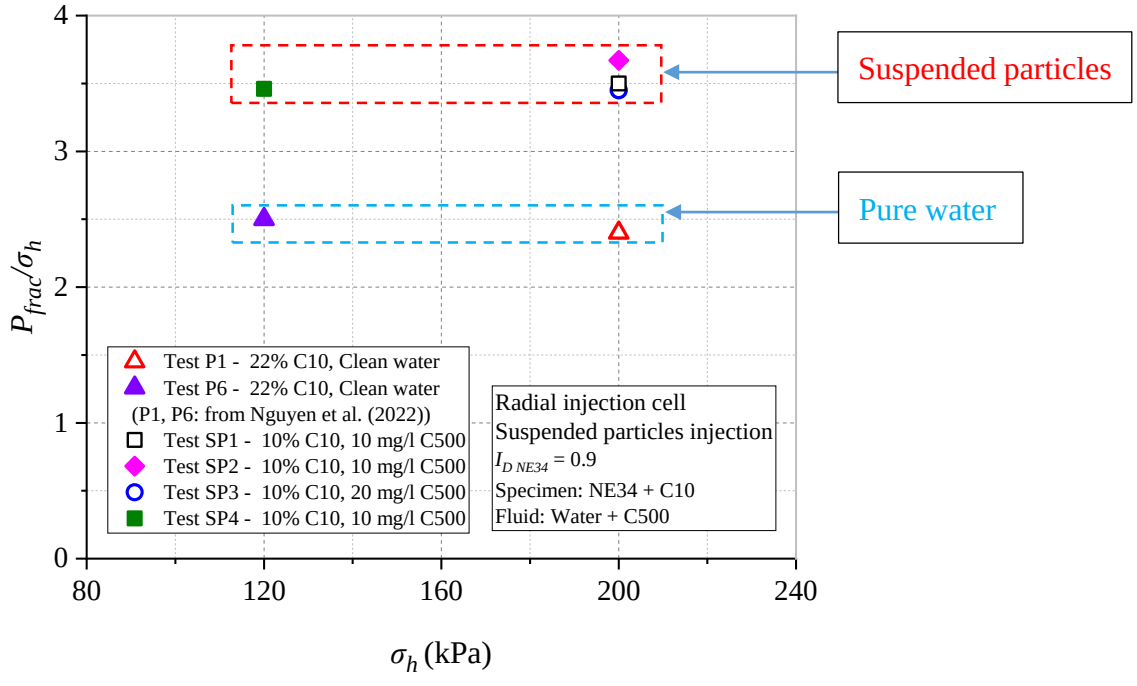

Fig. 21: Synthesis of the normalized fracturing pressure with the two scenarios: pure water and suspended particles injection.

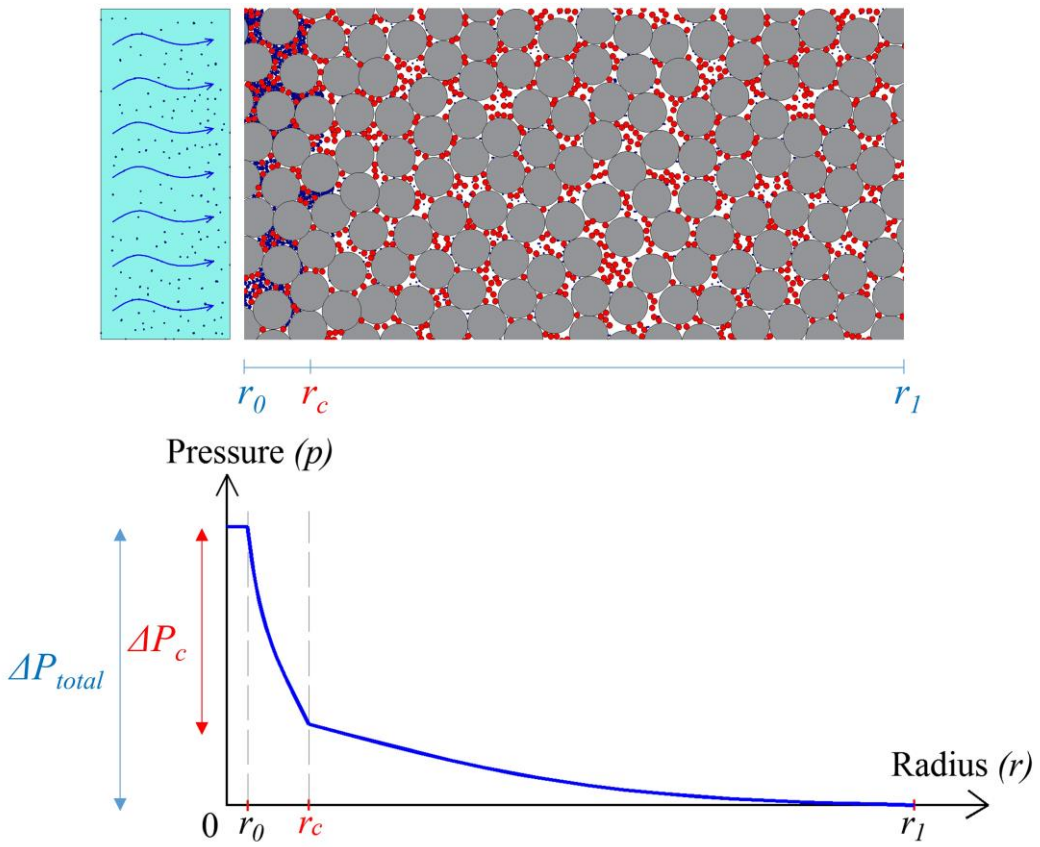

630

631 Fig. 22: Schematic representation of the pressure distribution within the clogged specimen by
632 entrance cake formation.

633

Material	D_{50} (μm)	C_u	e_{min}	e_{max}	Angularity	ρ_s (g/cm^3)
Fontainebleau NE34 sand	210	1.5	0.55	0.88	Sub-rounded	2.65
C10 fine particles	20	11	-	-	-	2.65
C500 fine particles	4.5	4.5	-	-	-	2.65

Table 1: Characteristics of the tested materials.

Section	Heigh (H)	Materials	Total mass (m)	$I_{D\ NE34}$	Porosity (n)	Dry density (ρ_d)
	cm	-	g	-	(%)	g/cm^3
Upper and lower layers of low permeability	2	NE34 + 32% C10	322	0.6	22	2.08
Injection zone	16	NE34 + 10% C10	2290	0.9	31	1.84

Table 2: Characteristics of the reference specimen.

Test	Fluid		Stress conditions			Density index of the matrix $I_{D\ NE34}$	Injection protocol
	μ (cP)	% C500 (mg/l)	σ_h (kPa)	σ_v (kPa)	K_0		
SP1	1	10	200	400	0.50	0.90	- Phase 1 (plugging phase) Injection at q = 0.2 l/min - Phase 2 (fracturing phase) Gradual increase of the flow rate until fracturing of the specimen
SP2	1	10	200	400	0.50	0.90	
SP3	1	20	200	400	0.50	0.90	
SP4	1	10	120	240	0.50	0.90	
SP5*	1	50	200	400	0.50	0.90	
SP6	1	50	200	400	0.50	0.90	

** test SP5 was performed with only the plugging phase*

Table 3: Characteristics of the sensitivity tests.